

NOTES

Limnol. Oceanogr., 46(1), 2001, 197–203
© 2001, by the American Society of Limnology and Oceanography, Inc.

Observations of a hydrothermal plume in a karstic lake

Abstract—A hydrothermal plume with vertical and horizontal length scales of ~ 18 and ~ 300 m, respectively, develops in a karstic lake. The plume is generated at the bottom of a basin that contains sediment in suspension, which is at a higher temperature than the water immediately above (the hypolimnion of the lake). The rising convective plume entrains colder hypolimnetic water and develops upward, until it reaches the base of the seasonal thermocline, carrying an important amount of sediment particles from the bottom, which are used as tracers to describe the spatial distribution of the plume. At the level of neutral buoyancy, the plume spreads laterally, as a horizontal baroclinic intrusion.

Lake Banyoles (located in Catalonia, northeast Spain), with a tectonic-karstic origin (Casamitjana and Roget 1993), is formed by six basins (CI–CVI), which are shown in Fig. 1. It is important to highlight that the entrance of water to the lake is through the bottom of these basins (via subterranean springs), mainly through CI (73.5 m deep), which is the biggest and supplies 85% of the total incoming water to the lake (500 L s^{-1}). The discharged volume by several creeks situated on the western shore of the lake is much smaller and depends on seasonal variations (Casamitjana et al. 1988; Roget et al. 1994; Colomer et al. 1998a).

The subterranean springs at the deep bottom of CI mix the sediments above, up to a fairly sharp sediment interface, known hereafter as the “lutocline” (Fig. 1). The lutocline is a strong gradient in density that divides the water column into two zones: a V-shaped zone below, full of sediments in suspension, and a zone of clearer water above. The zone of sediments in suspension has a vertical thickness of ~ 45 m, a sediment mass concentration of $\sim 120 \text{ g L}^{-1}$, and a temperature of $\sim 19.1^\circ\text{C}$, with only slight deviations measured throughout the year (Casamitjana and Roget 1993). The clear water, which is located above the lutocline, changes its temperature seasonally.

A two-dimensional seismic profile of CI and its interpretative section can also be seen in Fig. 1 (Canals et al. 1990). Here, the stratified-seismic response shows a flat signal at the lutocline (at a depth of ~ 30 m; Moreno-Amich and Garcia-Berthou 1989). During our field measurements, the lutocline was found to be at a depth of 29.2 m, as measured by portable sonar. Variations of the lutocline depth are attributed to variations of the groundwater discharge into the lake, in response to the changes of the precipitation in the recharge area (Casamitjana and Roget 1993).

The dynamics of the suspended sediment zone below the lutocline have been studied by Colomer et al. (1998a). Here, the formation of the lutocline was well predicted by a k - ϵ

model. This model shows that there is a strong mixing below the lutocline and a severe damping of the turbulent kinetic energy at the lutocline level. Therefore, the lutocline acts as a barrier to the propagation of the turbulent energy, and, as a consequence, at the lutocline level, the settling velocity of the suspension of particles is equal to the mean upward velocity.

The aim of this work is to assess that the dynamics of the water in the clear zone above the lutocline are governed by the convection caused by the difference in temperature between the suspension zone below the lutocline and the clearer zone above it. This difference in temperature induces the development of a turbulent convective plume, in the same way that turbulent convective plumes developed in localized sources (Maxworthy 1997) in oceanic and atmospheric deep convection (Schott et al. 1993, 1996), atmospheric microbursts (Lundgren et al. 1992), and urban heat islands (Lu et al. 1997a,b).

Microstructure, water quality, and particle-concentration data have been used to describe the vertical structure of the plume, as well as to track its spatial distribution in the hypolimnetic waters in the lake, with a total of six measurement stations, as shown in Fig. 1. Data are presented in an effort to support the presence of a hydrothermal plume that originated from a warm source. Results found from these field measurements (suspended particle-concentration and microstructure data) have also been found to be consistent with those found in the conceptual model known for these types of processes.

Methods—Several campaigns were performed during June 1998 at the center of CI (Sta. 1), along the main axis of the lake (Sta. 2, 4, and 6), and along the secondary axis of the lake (Sta. 3 and 5) (Fig. 1). Measurements of particle size distributions were performed with a laser in situ scattering and transmissometry probe (LISST-100), which works on the basis of laser diffraction to give information on particle size distribution and the particle volume concentration in a particle diameter range between 1.25 and $250 \mu\text{m}$. In addition to these primary parameters, LISST-100 gives information of the depth by means of a pressure sensor with a resolution of 5 cm. Moreover, secondary parameters, such as pH (± 0.2 units), dissolved oxygen concentration (accuracy $\pm 0.2 \text{ mg L}^{-1}$), redox potential (accuracy $\pm 20 \text{ mV}$), and conductivity (accuracy $\pm 0.001 \text{ mS cm}^{-1}$) were measured with a multiparametric probe (Hydrolab), to discriminate the type of particles present on the water column.

A profiler microstructure engine (PME) in downward mode collected microstructure data. The PME contains fast

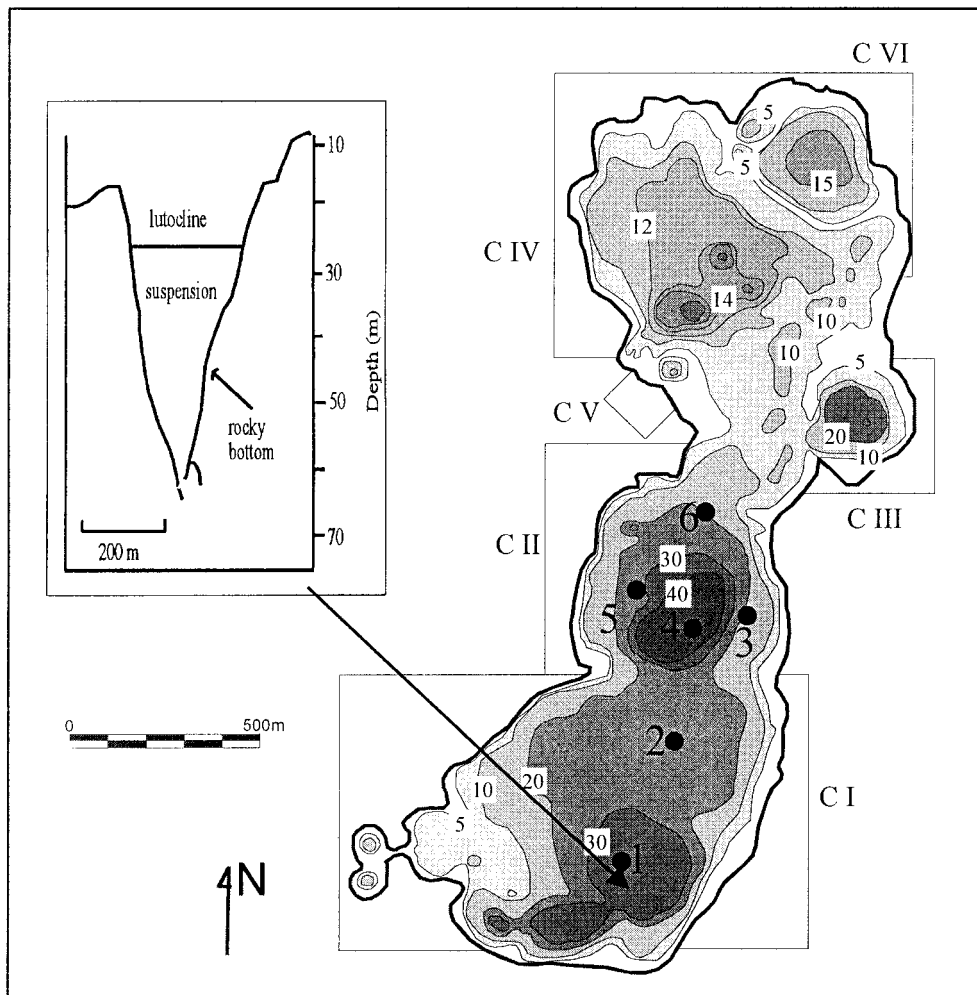


Fig. 1. Bathymetric map of lake Banyoles obtained from echosounding profiles (Moreno-Amich and Garcia-Berthou 1989). Depth contours are in meters. Numbers and points correspond to the measured field stations (from 1 to 6). Lake Banyoles is divided into six basins (CI–CVI). Water enters the lake from the bottom of these basins as underground springs. In basin I (CI), the maximum depth is ~ 75 m depth, although in the figure the lutocline is considered to be the virtual bottom (at ~ 30 m depth). Inset, seismic profiles and interpretative section of CI of Lake Banyoles.

time response sensors, to measure small-scale processes. It is composed of two thermistors (FP07, with a time response of 7 ms and a resolution of 0.01°C and a pressure sensor; Keller PSI PAA-10). To obtain the gradient signal, an electronic circuit derives the signals from the temperature sensors. The microprofiler sinks vertically at a speed of ~ 10 cm s^{-1} and samples at a frequency of 100 Hz; it therefore has a spatial resolution of ~ 1 mm. From the PME temperature-gradient spectra, dissipation rates are estimated by use of the Batchelor wave number method (Dillon and Caldwell 1980)—a technique based on segmenting the nonhomogeneous gradient profile into a set of homogeneous subrecords has been applied before the gradient spectra were computed (Imberger and Ivey 1991). Finally, the instantaneous structure of the plume can be enlightened from the Thorpe displacement values (d_T), which represent the vertical distance between the actual position of a fluid particle and its corresponding position in the synthetic stable profile of po-

tential density (Thorpe 1977; Luketina 1987). In this case, before computing d_T , the denoising wavelets procedure was applied to the recorded temperature profile (Donoho and Johnstone 1995).

Results—The water column above CI presents a summer-stratified water column with a well-developed epilimnion (from surface up to 6 m deep) and the thermocline below (with a vertical thickness of ~ 5 meters; see Fig. 2A). At the lutocline level, 29.2 m, the temperature increases up to 19.09°C . The temperature in the suspended sediment zone is not represented in Fig. 2A, but it was found to be constant downward and equal to 19.09°C . Details of the stratification can be observed from the temperature gradient signal (Fig. 2B), with mixing in the daily surface mixed layer and dominant positive temperature gradients within the thermocline (indicating its stability). Thorpe displacements (d_T) along depth at the center of basin CI show the highest values (of

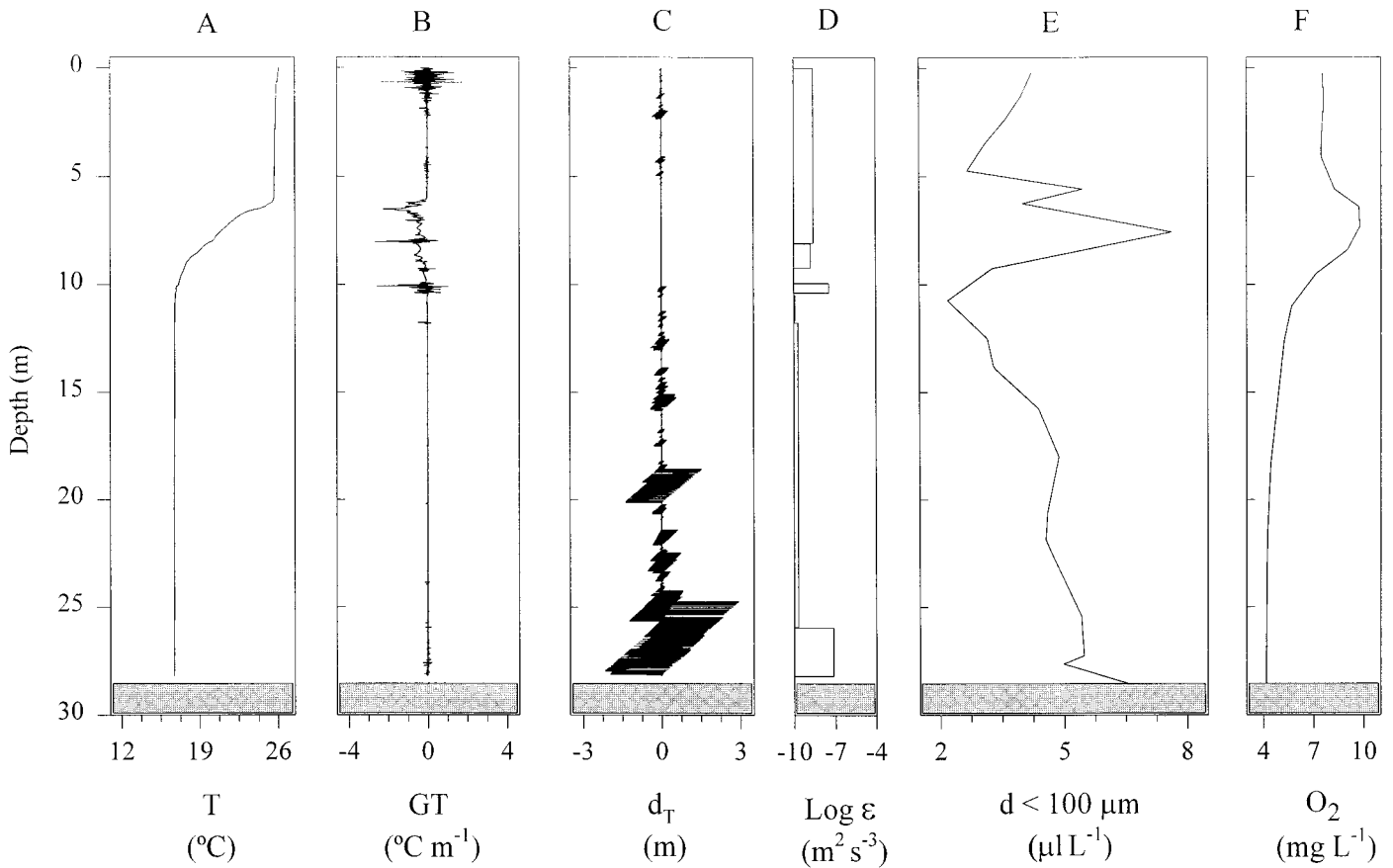


Fig. 2. Vertical profiles of (A) temperature, (B) temperature gradient, (C) Thorpe displacement, (D) logarithm of dissipation, (E) volume concentration of particles, and (F) dissolved oxygen concentration, in Sta. 1. A gray area at the bottom of each figure marks the lutocline depth.

about ± 2 m) at the base of the convective plume and decreasing upward (Fig. 2C). Negative and positive values of d_T indicate potential updrafts of warm fluid and downdrafts of cool fluid, respectively. It is also found that the dissipation of the turbulent kinetic energy, ϵ , at the base of the convective plume is 2 orders of magnitude higher than at the rest of the convective plume (Fig. 2D). All in all, there is a source of mechanical/thermal energy at the warm lutocline that is the basis for the development of the convective plume.

The hydrothermal plume carries a suspension of particles upward with particle volume concentrations of $\sim 5 \mu\text{L L}^{-1}$ immediately above the lutocline up to a depth of 15 m, then decreasing upward to $\sim 2.5 \mu\text{L L}^{-1}$ at a depth of 11 m (Fig. 2E). Within the thermocline (from 6 to 10 m), peaks of the particle-volume concentration of $\sim 7 \mu\text{L L}^{-1}$ and dissolved oxygen concentration (Fig. 2F) are attributed to an algal population (Garcia-Gil and Abella 1992).

As is expected from a convective plume, if the entrainment of the surrounding water takes place, the plume must reach a level of neutral buoyancy, at which height it must spread laterally (Whitehead et al. 1996; Colomer et al. 1998b). Detailed temperature microstructure profiles and corresponding temperature gradient signals and Thorpe dis-

placements outside the convective plume, at Sta. 2, show a horizontal intrusion at depths between 14.6 and 15.8 m (Fig. 3). The intrusion, i.e., the spreading current originated at CI, carries a signal of particles that was detected at Sta. 2 and 3 (Fig. 4). These peaks of particle-volume concentration were found to extend to a wider range (12–19 m) than the temperature intrusion (14.6–15.8 m). The dispersion and sedimentation of particles from the spreading current might cause this difference. Also, the sedimentation of algae from the thermocline might also contribute to. At Sta. 6, situated at the longest distance from the plume source, the particle concentration is larger at ~ 19 m. This clearly indicates that particles are settling down from the intrusion.

Volume samples of 5 liters were taken at different depths in Sta. 1, to elucidate the nature of the particles. Samples were filtered in glass-fiber filters, dried, and later muffled at a 500°C (as detailed by Kristensen and Andersen 1987). From the difference between the mass of the samples before and after being muffled, the organic matter could be quantified. The solid mass of the 12-m depth sample is composed of 50% organic matter and 50% inorganic matter. In addition, the percentage of inorganic matter increased with depth—that is, at a depth of 15 m, the mass concentration was 95% inorganic matter and 5% organic matter, and the

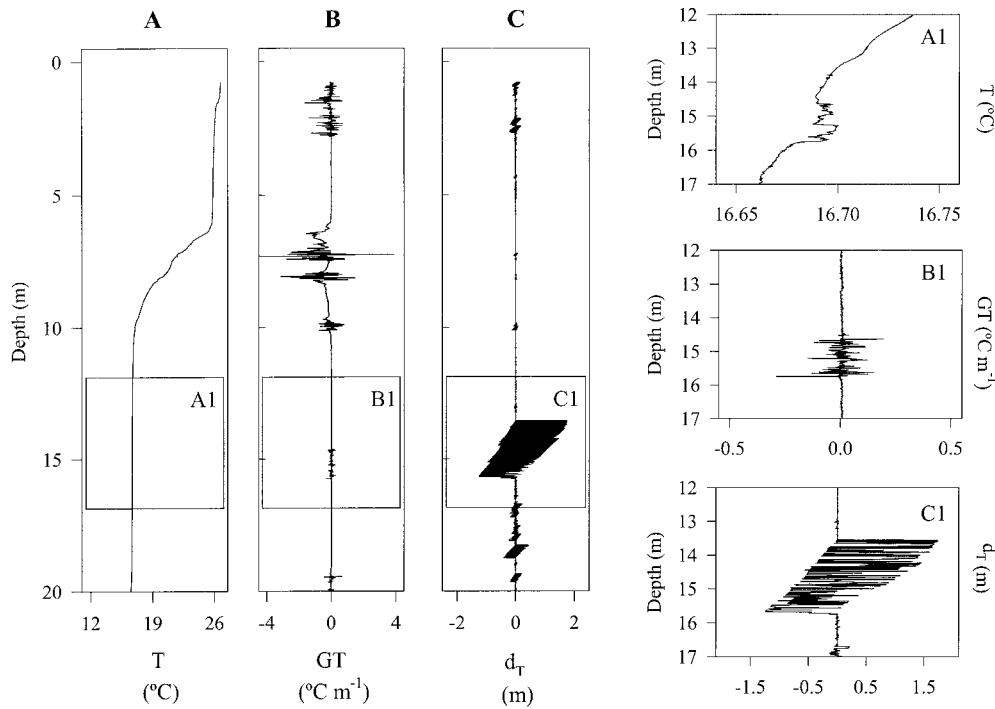


Fig. 3. Vertical profiles of (A) temperature, (B) temperature gradient, and (C) Thorpe displacements, in Sta. 3. Details of these measurements (between 12 and 17 m) can be seen in the boxes of amplified results, on the right (A1, B1, and C1).

composition remains constant hereafter. Also, there was no variation in dissolved oxygen concentration, redox potential, pH, and conductivity at the depth at which the spreading current was detected. Therefore, the signal is attributed to

inorganic particles, which ought to be advected from its unique source: the convective plume over the lutocline in CI.

A peak of the particle-volume concentration was found at different stations of the lake (Sta. 1, 2, and 3) at the spreading level (~15 m) (see Fig. 1). This peak of particles was not found in Sta. 4 and 5, as shown in Fig. 4; the particle-concentration profiles show almost no signal of particles at Sta. 4 and 5. Therefore, the current seems to deviate toward the northeast of the lake. Finally, the particles carried out by the spreading current were found to settle down at Sta. 6, where a typical settling particle-concentration profile was found to have larger concentrations at the bottom (at 18.5 m deep) that decreased exponentially upward (see also Fig. 4).

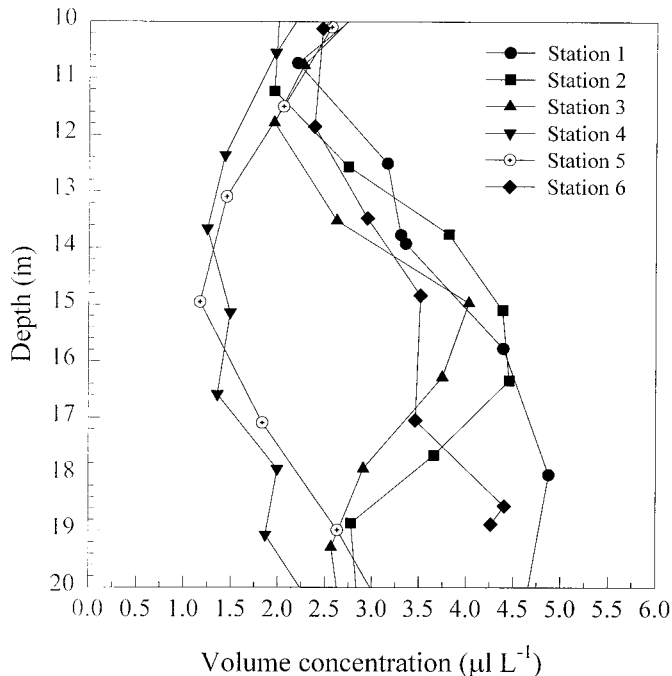


Fig. 4. Vertical profiles of volume particle concentration at Sta. 1-6 at depths of interest.

Discussion—At the lutocline level, the mean upward velocity and momentum are not zero because of the entering groundwater. Therefore, it is crucial to elucidate whether the originated buoyant jet is plumelike or jetlike. This can be determined by means of the characteristic length scale $l_m = M_o^{3/4}/Q_o^{1/2}$ (Fischer et al. 1979), which is the balance between the momentum flux (M_o) and the total buoyancy flux (Q_o). M_o is defined as $\pi D^2 w_o^2/4$ (D is the diameter of the source, and w_o is the vertical velocity of the fluid), and Q_o is defined as $\pi D^2 \Delta b_o w_o/4$, where Δb_o is the buoyancy of the resulting discharge, defined as $\Delta b_o = (\rho_p - \rho_o)g/\rho_o$. ρ_p and ρ_o are the densities of the water discharge and the background fluid, respectively, and g is the gravitational acceleration. As a result, the buoyant jet will be jetlike for vertical distance $z < l_m$ —i.e., momentum forces are dominant, compared with the buoyancy forces. On the contrary, for vertical distances,

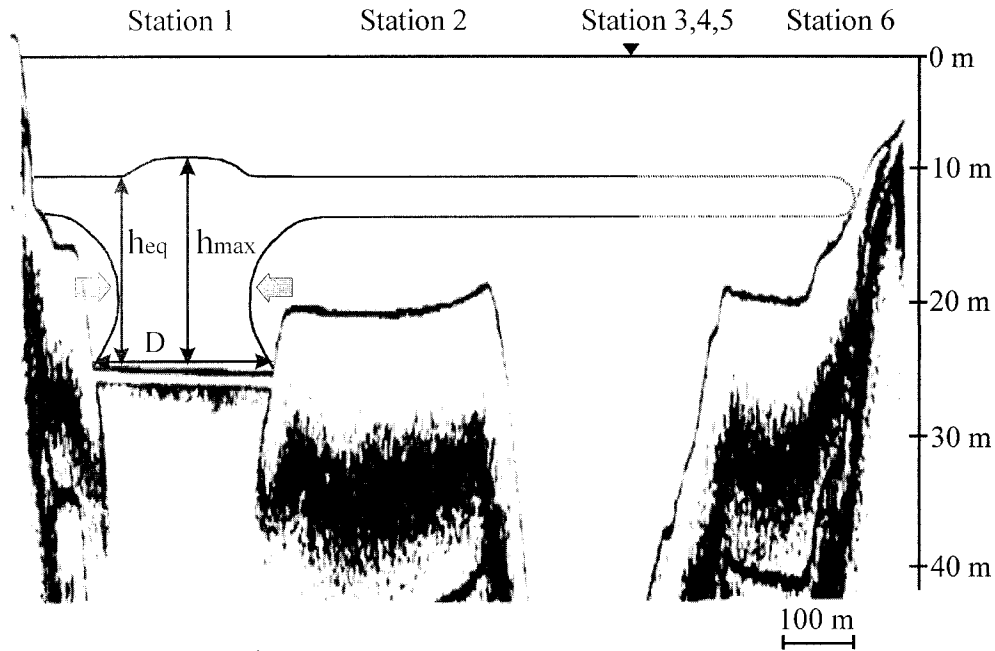


Fig. 5. Schematic view of the hydrothermal plume, with a source diameter, D , plotted on the seismic profile done by Canals et al. (1990). The convective plume reaches an equilibrium height h_{eq} , and the vertical excursion stops at a height h_{max} (h_{max} and h_{eq} are defined from the plume source depth, Eqs. 1 and 2). Vertical and horizontal scales are in meters.

$z > l_m$, the buoyant jet will be plume-like—i.e., buoyant forces are higher than momentum forces. When $w_o \sim 10^{-5} \text{ ms}^{-1}$ and $D \sim 300 \text{ m}$ (Casamitjana and Roget 1993) are considered, values of $Q_o \sim 2.5 \times 10^{-3} \text{ m}^4 \text{ s}^{-3}$ and $M_o \sim 7.1 \times 10^{-6} \text{ m}^4 \text{ s}^{-2}$ were found; therefore, $l_m = 0.28 \text{ cm}$, which shows that buoyancy forces dominate from very short distances above the source. This means that the flow is plume-like.

Under the assumption that the plume is in the quasi steady state, several nondimensional numbers describe the system in which the stratification and size of the forcing region (the lutocline) are included (Maxworthy and Narimousa 1994; Whitehead et al. 1996; Maxworthy 1997). The nondimensional number N/f compares the relative significance between stratification (through N) and rotation (through f , the rotation rate). For the case in hand, $N = 4.4 \times 10^{-3} \text{ s}^{-1}$, and $f = 9.75 \times 10^{-5} \text{ s}^{-1}$; thus, $N/f = 45$ —i.e., the stratification is stronger than the rotation. Another significant nondimensional number is the aspect ratio of the plume (A_p), which is defined as the ratio between the vertical maximum height of the plume (h_{max} , which will be calculated later on the text; see Eq. 1) and the horizontal source diameter (D ; see scheme in Fig. 5). In our case, $A_p = h_{max}/D = 0.06$, which is in the range of plumes with low aspect ratios. Examples of large A_p are found in point-plume sources, whereas examples of low aspect ratios are found in geophysical applications, such as urban heat islands ($A_p \sim 0.06$; Colomer et al. 1999), the Central Labrador deep ocean convection ($A_p \sim 0.01$; Sy et al. 1997), the Gulf of Lion deep ocean convection ($A_p \sim 0.02$ – 0.03 ; Gaillard and Desaubies 1997), and the Juan de Fuca Ridge megaplume ($A_p \sim 0.05$; Baker et al. 1987). Finally, the Rossby plume number, $R_o^* = (B_o/f^3 h_o^2)^{1/2}$ deter-

mines whether the plume develops a single vortex column or several vortices (Maxworthy and Narimousa 1994). B_o is the total buoyancy flux per unit area, f is the Coriolis parameter, and h_o is the length scale of convection. On the basis of the maximum height to which the hydrothermal plume can rise, a value of $R_o^* = 6.5$ was found, which is 1 order of magnitude larger than those found in oceanic regions that experience deep convection (Whitehead et al. 1996) and is smaller than typical values found in the atmosphere (Colomer et al. 1999). The value of $R_o^* = 6.5$ calculated for the Lake Banyoles plume corresponds to the range in which a convective plume develops a single vortex column (Narimousa 1996).

Different laboratory experimental works have been carried out in order to evaluate the most important quantities that characterize the plume structure, such as the maximum height (h_{max}) to which the plume migrates and the equilibrium height (h_{eq}), at which the plume spreads laterally. Both h_{max} and h_{eq} have been found to be functions of the characteristics of the source (D , B_o), the stratification of the water column (N), and the rotation rate (f) (Whitehead et al. 1996; Maxworthy 1997). h_{max} is determined by the height at which the plume is arrested by lateral buoyancy flux because of baroclinic eddies, i.e.,

$$h_{max} = 3.7(B_o D)^{1/3}/N, \quad (1)$$

where the value 3.7 is obtained from laboratory experiments, with the interesting result that h_{max} is independent of rotation (Whitehead et al. 1996). In addition, recent results show that $h_{eq}/h_{max} = 0.694$ (Lu et al. 1997a), in which case the plume reaches its level of neutral buoyancy and spreads laterally at a height

$$h_{\text{eq}} = 2.6(B_0 D)^{1/3}/N. \quad (2)$$

Finally, the number of vortices that are formed by the baroclinic instability (Whitehead et al. 1996) can be calculated by use of the following:

$$N_v = 0.7(D^2/B_0)^{1/3}f. \quad (3)$$

If $Q_0 \sim 2.5 \times 10^{-3} \text{ m}^4 \text{ s}^{-3}$ and $D \sim 300 \text{ m}$ (Fig. 4), then $B_0 = 3.5 \times 10^{-8} \text{ m}^2 \text{ s}^{-3}$. Furthermore, if $N = 4.4 \times 10^{-3} \text{ s}^{-1}$, as is obtained from high-precision temperature profiles, the $h_{\text{max}} = 18.4 \text{ m}$, $h_{\text{eq}} = 13.0 \text{ m}$, and $N_v = 0.94 \sim 1$ are obtained from Eqs. 1, 2, and 3, respectively. Then the maximum and equilibrium heights are located at 10.8 and 16.2 m from the surface, respectively. This calculated result, h_{max} , has been found to be coincident with the measured depth at which the particle concentration showed a minimum, and then increased downward by the lutocline (Fig. 2E). Moreover, h_{eq} is also in accordance with the depth at which the intrusion was detected by means of the microstructure data from the temperature gradient (Fig. 3).

Finally, the Richardson number, $Ri = g'h_0/(B_0 R)^{2/3}$ —where g' is the reduced gravity across the density interface, h_0 is the depth of the convective layer, and R is the radius of the source—it can be used to determine whether the plume will penetrate through the thermocline (Narimousa 1996). A value of $Ri \sim 200$ was found, which is larger than the critical Richardson number, $Ri_c \sim 11$, above which it is found that convective flows do not penetrate through density interfaces (Narimousa 1996).

More research should be done to assess whether this hydrothermal plume is always present in the lake. In that case, the plume would be termed a “chronic plume” (Palmer and Ernst 1998). Furthermore, it would be interesting to check the characteristics of the plume for different environmental conditions of the water column, such as the winter mixed period. More field experiments should be also done to corroborate experimentally whether only one vortex is generated around the plume, as theory predicts.

Indeed, the plume described in this paper might alter significantly different aspects of the lake, such as possible interpretations of lake sedimentary structures around CI and, therefore, paleoclimate inferences obtained from sedimentary cores. It can be expected that suspended particles change the clarity of the water, which might determine the biology of the lake. For example, fishes might constrain their habitat as a function of the clarity of the water for their feeding opportunities and other visual activities (Moyle and Cech 1996; Mathews 1998; García-Berthou 1999).

Conclusions—Temperature and particle-concentration measurements demonstrate the presence of a hydrothermal plume generated because of the higher temperature of a localized suspended sediment bottom, compared with its surroundings, in a tectonic-karstic lake. The advancing particle-laden plume, which carries particles from the sediments suspended at the bottom, develops upward until it reaches the level of neutral buoyancy ($\sim 15 \text{ m}$ depth), spreading laterally as a gravity current. The estimated value of the Rossby plume number ($Ro^* = 6.5$) shows that rotation affects the plume development. It was also found that the plume de-

velops to a maximum height limited by the strong temperature gradient of the seasonal thermocline.

It is expected that the hydrothermal plume might also affect the general circulation and water quality of the lake. It might also play an important role in determining the biology of the lake. This study, together with other studies, such as atmospheric and oceanic deep convection, contribute to the general and detailed understanding of the development of the convection process from a finite isolated source in different environments.

Jordi Colomer¹
Teresa Serra
Jaume Piera
Elena Roget
Xavier Casamitjana

Department of Physics
University of Girona
Campus de Montilivi
17071 Girona, Spain

References

- BAKER, E. T., G. J. MASSOTH, AND R. A. FEELY. 1987. Cataclysmic hydrothermal venting on the Juan de Fuca Ridge. *Nature* **329**: 149–151.
- CANALS, M., H. GOT, R. JULIA, AND J. SERRA. 1990. Solution-collapse depressions and suspensates in the limnogenic lake of Banyoles (NE Spain). *Earth Surface Proc. Landforms* **15**: 243–254.
- CASAMITJANA, X., AND E. ROGET. 1993. Resuspension of sediment by focused groundwater in Lake Banyoles. *Limnol. Oceanogr.* **38**: 643–656.
- , ———, D. JOU, AND J. E. LLEBOT. 1988. Effect of the suspended sediment on the heating of Lake Banyoles. *J. Geophys. Res.* **93**: 9332–9336.
- COLOMER, J., B. M. BOUBNOV, AND H. J. S. FERNANDO. 1999. Turbulent convection from isolated sources. *Dynam. Atmos. Oceans* **30**: 125–148.
- , J. A. ROSS, AND X. CASAMITJANA. 1998a. Sediment entrainment in karst basins. *Aquat. Sci.* **60**: 338–358.
- , L. D. ZIEREN, AND H. J. S. FERNANDO. 1998b. Comment on “Localized convection in rotating stratified fluid” by J. A. Whitehead et al. *J. Geophys. Res.* **103**: 12,891–12,894.
- DILLON, T. M., AND D. R. CALDWELL. 1980. The Batchelor spectrum and dissipation in the upper ocean. *J. Geophys. Res.* **85**: 1910–1916.
- DONOHO, D. L., AND I. M. JOHNSTONE. 1995. Adapting to unknown smoothness via wavelet shrinkage. *J. Am. Stat. Assoc.* **90**: 1200–1224.
- FISCHER, H. B., E. J. LIST, R. C. Y. KOH, J. IMBERGER, AND N. H. BROOKS. 1979. Mixing in inland and coastal waters. Academic.
- GAILLARD, F., AND Y. DESAUBIES. 1997. A four-dimensional analysis of the thermal structure in the Gulf of Lion. *J. Geophys. Res.* **102**: 12,515–12,537.
- GARCÍA-BERTHOU, E. 1999. Spatial heterogeneity in roach (*Rutilus*

¹ Corresponding author (colomer@inferr.udg.es).

Acknowledgements

We would like to thank Antoine Avignon and the captain, Joan Corominas, for their help during the field campaign. We also acknowledge the comments of two anonymous reviewers, which helped to improve the paper considerably.

- rutilus*) diet among contrasting basins within a lake. *Arch. Hydrobiol.* **145**: 239–256.
- GARCIA-GIL, L. J., AND C. A. ABELLA. 1992. Population dynamics of phototrophic bacteria in three basins of lake Banyoles (Spain). *Hydrobiologia* **243**: 87–94.
- IMBERGER, J., AND G. N. IVEY. 1991. On the nature of turbulence in a stratified fluid. Part II: Application to lakes. *J. Geophys. Res.* **21**: 659–680.
- KRISTENSEN, E., AND ANDERSEN, F. 1987. Determination of organic carbon in marine sediments: A comparison of two CHN-analyser methods. *J. Exp. Mar. Biol. Ecol.* **109**: 15–23.
- LU, J., S. P. ARYA, W. H. SNYDER, AND R. E. LAWSON, JR. 1997a. A laboratory study of the urban heat island in a calm and stably stratified environment. Part I: Temperature field. *J. Appl. Meteorol.* **36**: 1377–1391.
- , ———, ———, AND ———. 1997b. A laboratory study of the urban heat island in a calm and stably stratified environment. Part II: Velocity field. *J. Appl. Meteorol.* **36**: 1392–1402.
- LUKETINA, D. A. 1987. Frontogenesis of freshwater overflows. Ph.D. thesis, University of Western Australia, Nedlands.
- LUNDGREN, T. S., J. YAO, AND N. N. MANSOUR. 1992. Microburst modelling and scaling. *J. Fluid Mech.* **239**: 461–483.
- MATHEWS, W. J. 1998. Patterns in freshwater fish ecology. Chapman & Hall.
- MAXWORTHY, T. 1997. Convection into domains with open boundaries. *Annu. Rev. Fluid Mech.* **29**: 327–371.
- , AND S. NARIMOUSA. 1994. Unsteady turbulent convection into a homogeneous rotating fluid, with oceanographic applications. *J. Phys. Oceanogr.* **24**: 865–887.
- MORENO-AMICH, R., AND E. GARCIA-BERTHOU. 1989. A new bathymetric map based on echosounding and morphological characterization of the Lake Banyoles. *Hydrobiologia* **185**: 83–90.
- MOYLE, P. B., AND J. J. CECHE, JR. 1996. Fishes: An introduction to ichthyology. Prentice Hall.
- NARIMOUSA, S. 1996. Penetrative turbulent convection into a rotating two-layer fluid. *J. Fluid Mech.* **321**: 299–313.
- PALMER, M. R., AND G. G. J. ERNST. 1998. Generation of hydrothermal megaplumes by cooling of pillow basalts at mid-ocean ridges. *Nature* **393**: 643–647.
- ROGET, E., X. CASAMITJANA, AND J. E. LLEBOT. 1994. Calculation of the flow into a lake from underground springs using sedimentation rates. *Neth. J. Aquat. Ecol.* **28**: 135–141.
- SCHOTT, F., M. VISBECK, AND J. FISCHER. 1993. Observations of vertical currents and convection in the central Greenland Sea during the winter of 1988/89. *J. Geophys. Res.* **98**: 14,401–14,421.
- , ———, U. SEND, J. FISCHER, L. STRAMMA, AND Y. DESAUBIES. 1996. Observations of deep convection in the Gulf of Lions, Northern Mediterranean, during the winter of 1991/92. *J. Phys. Oceanogr.* **26**: 505–524.
- SY, A., M. RHEIN, J. R. N. LAZIER, K. P. KOLTERMANN, J. MEINCKE, A. PUTZKA, AND M. BERSCH. 1997. Surprisingly rapid spreading of newly formed intermediate waters across the North Atlantic Ocean. *Nature* **386**: 675–679.
- THORPE, S. A. 1977. Turbulence and mixing in a Scottish loch. *Philos. Trans. R. Soc. London Ser. A Math. Phys. Sci.* **286**: 125–181.
- WHITEHEAD, J. A., J. MARSHALL, AND G. E. HUFFORD. 1996. Localized convection in rotating stratified fluid. *J. Geophys. Res.* **101**: 25,705–25,721.

Received: 15 October 1999
Accepted: 8 August 2000
Amended: 25 September 2000

A high-resolution pore water sampler for sandy sediments

Abstract—In this paper, we present a new technique for collecting pore-water samples in coarse- to fine-grained sandy sediments. We have used the technique both for in situ sampling and for pore-water extraction from sediment cores brought back to the laboratory, in both cases with a depth resolution as fine as 1 cm. The key device is a long, thin (~2 mm) stainless steel tube with a specially designed tip that functions as a filter. Pore-water samples are collected by inserting the tube into the sediment at the desired depth and applying a light suction from a syringe connected to the tube. The sample is injected immediately into a vial through a syringe filter and stored for later analysis. The technique has some clear advantages over other methods that are used commonly in sandy sediments. In comparison with lysimeters or sippers, it gives pore-water samples with a much higher depth resolution, which often is needed to accurately estimate fluxes across the sediment-water interface or transformation rates of solutes within the sediments. In comparison with dialysis cells or peepers, the new technique gives measurements that truly represent the time of collection. This can be crucial when non-steady-state systems are studied. Furthermore, disturbance of the sediment is minimal because of the small dimension of the tube. This is especially important in vegetated sediments, in which the deployment of larger conventional samplers is likely to cause significant disturbance. Finally, sample extraction is

less laborious than other techniques, requiring only one site visit and typically <1 min of sampling time per sample. In laboratory tests using a dye tracer, we showed that pore water was drawn evenly toward the tube tip from all directions in the surrounding sediment. On the basis of these results, we provide guidelines for choosing the appropriate sampling depth intervals as a function of the sample size. Data from representative pore-water profiles are presented for PO_4^{3-} from vegetated coarse-grained carbonate sediments in the Bahamas and NH_4^+ from fine-grained unvegetated sands in a temperate coastal lagoon in Virginia.

Concentration profiles of pore water in sediments are used extensively in studies of biogeochemical processes. Vertical gradients of pore-water solutes have been used to calculate fluxes across the sediment-water interface (Glud et al. 1995; Charpy-Roubaud et al. 1996; Urban et al. 1997). Furthermore, estimates of carbon, nitrogen, and phosphorus transformations within the sediments, such as mineralization, denitrification, and benthic photosynthesis, can be obtained from the profile curvature (Revsbech et al. 1981; Dalsgaard and Revsbech 1992; Berg et al. 1998; McGlathery et al. pers. comm.). Microelectrodes (Revsbech et al. 1980) provide an